GEOPHYSICS, VOL. 72, NO. 4 (JULY-AUGUST 2007); P. N11–N21, 7 FIGS., 3 TABLES.
10.1190/1.2740666

P-wave seismic attenuation by slow-wave diffusion: Numerical experiments in partially saturated rocks

Stefano Picotti[1], José M. Carcione[1], J. Germán Rubino[2], and Juan E. Santos[3]

ABSTRACT

P-wave attenuation by slow-wave diffusion is a significant loss mechanism at seismic frequencies. This effect is known as mesoscopic loss, because it is a consequence of fluid flow at mesoscopic-scale inhomogeneities. These are larger than the pore size but smaller than the wavelength, typically tens of centimeters, and are due to local variations in lithological properties or to patches of immiscible fluids. Basically, a P-wave traveling in a porous medium induces a fluid-pressure gradient in regions of different properties, such as patches saturated with different fluids, generating slow P-waves, which diffuse away from the interfaces separating the fluids. This mechanism can be explained by the combined effect of mesoscopic-scale inhomogeneities and mode conversion at interfaces. We consider a periodically stratified medium and perform numerical experiments to determine the P-wave quality factor in partially saturated rocks. The modeling method is an iterative domain-decomposition 2D finite-element algorithm for solving Biot equations of motion in a parallel computer, which is a requirement to run the numerical experiments at seismic frequencies. The simulated pulses show evidence of the mesoscopic-loss mechanism, and the quality factors estimated with the spectral-ratio and frequency-shift methods are in good agreement with the theoretical values predicted by the White theory. Errors in the estimation of the quality factor are less than 5% (spectral ratio) and 3% (frequency shift).

INTRODUCTION

Recent studies (Pride et al., 2002, 2004; Müller and Gurevich, 2005; Carcione and Picotti, 2006) have shown that the major cause of attenuation at seismic frequencies in porous media is wave-induced fluid flow, which arises when a wave induces gradients of fluid pressure in regions of rock saturated by different fluid types, or when the rock is heterogeneous. In particular, Carcione and Picotti (2006) investigate the amount of attenuation and velocity dispersion caused by different types of heterogeneities in the rock properties; namely, porosity, grain and frame moduli, permeability, and fluid properties. The analysis indicates that the most effective loss mechanisms are a result of porosity variations and partial saturation, where one of the fluids is very stiff and the other is very compliant. An example of such a medium is a highly permeable sandstone at shallow depths that is saturated with water and small amounts of gas (around 10% saturation). The physics are basically energy conversion from the fast P-wave into the slow P-wave, which is a diffusive (static) mode at seismic frequencies. This effect occurs at different spatial scales; at seismic frequencies the size of the inhomogeneities is on the order of centimeters.

The macroscopic nature of the attenuation mechanism was first investigated by Biot in several classical papers (Biot, 1956a, b, 1962). Biot's theory of wave propagation predicts that, besides the existence of a fast P-wave and an S-wave, a slow P-wave can occur in partially saturated porous media. This wave, which behaves as a diffusion mode, has been detected under very specific laboratory conditions on synthetic samples (Plona, 1980; Chin et al., 1985; Smeulders, 2005). However, laboratory measurements point out that the attenuation levels predicted by the macroscopic-flow mechanism underestimate the velocity dispersion and attenuation in rocks (e.g., Mochizuki, 1982; Dvorkin et al., 1995; Arntsen and Carcione, 2001).

A range of models have been proposed to investigate the microscopic nature of attenuation. These models are based on the so-called local fluid flow, or "squirt" flow absorption mechanisms (O'Connell and Budiansky, 1974; Dvorkin et al., 1995; Mavko et al., 1998), which seem to give good qualitative predictions as a function of the fluid viscosity. In these mechanisms, fluid-filled microcracks re-

Manuscript received by the Editor August 11, 2006; revised manuscript received March 1, 2007; published online June 27, 2007.
[1]Istituto Nazionale di Oceanografia e di Geofisica Sperimentale (OGS), Trieste, Italy. E-mail: spicotti@ogs.trieste.it; jcarcione@ogs.trieste.it.
[2]Universidad Nacional de La Plata, CONICET, Departamento de Geofísica Aplicada, Facultad de Ciencias Astronómicas y Geofísicas, La Plata, Argentina. E-mail: grubino@fcaglp.fcaglp.unlp.edu.ar.
[3]Universidad Nacional de La Plata, CONICET, Departamento de Geofísica Aplicada, Facultad de Ciencias Astronómicas y Geofísicas, La Plata, Argentina and Purdue University, Department of Mathematics, West Lafayette, Indiana. E-mail: santos@fcaglp.fcaglp.unlp.edu.ar.

spond with greater fluid-pressure changes than the main pore space. The resulting flow at this microscopic level is responsible for the energy loss. The models have the proper dependence on viscosity, but the mechanism is incapable of describing the measured levels of dissipation at seismic frequencies (Diallo et al., 2003; Pride et al., 2004).

White and coauthors (White, 1975; White et al., 1975) are the first to show that significant amounts of seismic wave attenuation can occur at seismic frequencies in a partially saturated porous rock. They introduce the mesoscopic-loss mechanism and give an approximate theory for the calculation of attenuation and dispersion of P-waves in porous rocks saturated with brine and gas. This is the first so-called "patchy saturation" model, which describes a very common configuration in sedimentary rocks. For instance, regions of nonuniform patchy saturation occur at gas-oil and gas-water contacts in hydrocarbon reservoirs. Also, during production, gas may come out of solution and create pockets of free gas. When sonic logs are used to infer the behavior of acoustic properties at seismic frequencies, the mesoscopic-loss effect becomes important. The mesoscopic-scale length is intended to be much larger than the grain sizes but much smaller than the wavelength of the pulse. As demonstrated by White (1975), partial saturation induces wave-velocity dispersion and attenuation, which depends mostly on the size of the gas pockets (saturation), frequency, permeability, and porosity of the rocks. A fast P-wave traveling in the medium induces a greater fluid pressure in the gas patches than in the water-saturated parts of the material. This in turn generates fluid flow and slow Biot waves, which diffuse away from the gas-water interfaces, generating significant losses in the seismic range.

The mesoscopic-loss theory has been further refined by other researchers. Dutta and Seriff (1979) modify White's equations in the case of spherical gas-filled patches, bringing the results into good agreement with the more exact calculations of Dutta and Odé (1979a, b), who solve the problem exactly in the frame of Biot theory. In particular, the modified equations give the expected Gassmann-Wood velocity at very low frequencies. Dutta and Seriff (1979) also compare the results obtained using three different geometries of the patches, and conclude that the geometry configuration has no important effect on the magnitude of attenuation. In recent studies (Johnson, 2001; Müller and Gurevich, 2004a, b) a generalization of the White model for patches of arbitrary shape is developed. Besides the usual parameters of Biot theory, these models have other geometrical parameters, for example, the specific surface area and the size of the patches (Johnson, 2001). Müller and Gurevich (2004b) compare attenuation and dispersion predictions obtained from the periodic model of White (1975) to those generated from a 3D model with any type of random inhomogeneity. They find that, even if the attenuation peak for the random model is broader and smaller than that of the periodic model, the frequency dependency of attenuation and velocity are very similar. In particular, if ω is the angular frequency, the predicted dissipation factor $1/Q$ for the random model is proportional to ω and $1/\sqrt{\omega}$ at the low- and high-frequency limits, respectively, which is the same as the periodic model. This means that, qualitatively, the effects of geometry are not significant.

Other important works on the subject are Norris (1993), Gurevich and Lopatnikov (1995), Gelinsky and Shapiro (1997), Gurevich et al. (1997), and Shapiro and Müller (1999). Carcione and Picotti (2006) provide an extensive overview of the mesoscopic-loss literature. They use the first model proposed by White (1975), i.e., a periodically layered porous medium saturated with water and gas for their estimations of quality factor Q and velocity dispersion. The quality factor Q as well as traveltime, wave phase, and polarization, is a fundamental seismic indicator for the evaluation of in-situ rock properties, particularly fluid type, permeability, and porosity. Gurevich et al. (1997) obtain the P-wave quality factor as a function of frequency for 1D finely layered poroelastic media (normal to layering). They consider Biot loss, scattering, and mesoscopic-flow loss and find that the quality factor is approximately given by the harmonic average of the corresponding single quality factors.

Carcione et al. (2003) perform numerical modeling experiments based on Biot equations of poroelasticity and the White model of regularly distributed spherical gas inclusions. They show that attenuation and velocity dispersion measurements can be explained by the combined effect of mesoscopic-scale inhomogeneities and energy transfer between wave modes. By using computerized tomography (CT) scans it is possible to visualize the fluid distribution and spatial heterogeneities in real rocks (Cadoret et al., 1995). Fractal models, such as the von Kármán correlation function, calibrated by the CT scans, are used by Helle et al. (2003) to model heterogeneous rock properties and perform numerical experiments based on Biot equations of poroelasticity.

In this work we consider the model used in Carcione and Picotti (2006) to test the numerical-modeling algorithm for computing realistic synthetic seismograms. We compare the analytical and numerical phase velocities and loss angles (related to the quality factor) obtained in two cases of partial saturation. This model is very useful because it is mathematically simple and allows us to model different mesoscopic-scale heterogeneities. Since the geometry of the gas-filled patches is not really very important for the evaluation of attenuation (Johnson, 2001; Müller and Gurevich, 2004a,b), the qualitative aspects of the physics obtained using this model have a general validity. The modeling algorithm is a parallel and iterative finite-element domain-decomposition method to solve Biot's equation of motion at seismic frequencies. The algorithm uses a nonconforming rectangular element (Douglas et al., 1999) to approximate the displacement vector in the solid phase, which allows a reduction in the number of points per wavelength necessary to reach a desired accuracy (Zyserman et al., 2003). Compared with the corresponding procedure using conforming elements of the same order, this method considerably reduces the amount of information exchanged in any parallel implementation of the algorithm. The synthetic time histories show clearly the mesoscopic-loss mechanism due to the slow-wave diffusion, and the observed attenuation levels are in very good agreement with those predicted by White theory.

BIOT THEORY

The propagation of waves in a porous elastic solid saturated by a single–phase compressible viscous fluid was first analyzed by Biot in two important classic papers (Biot, 1956a, b). He considered a porous isotropic medium and assumed that the fluid may flow within the solid frame causing friction to arise. Let $\mathbf{u}^f = \phi(\widetilde{\mathbf{u}}^f - \mathbf{u}^s)$ be the average relative fluid displacement per unit volume of bulk material, where $\mathbf{u}^s$ and $\widetilde{\mathbf{u}}^f$ denote the averaged solid and fluid displacement vectors, respectively, and ϕ is the porosity. Also, set $\mathbf{u} = (\mathbf{u}^s, \mathbf{u}^f)$ and note that the change in fluid content per unit volume is given by $\xi = -\nabla \cdot \mathbf{u}^f$. Finally, let σ_{ij}, $i,j = 1, \ldots, d_e$, and p_f denote, respectively, the stress tensor of the bulk material and the fluid pressure, where d_e is the Euclidean dimension. Following (Biot, 1962), the stress-strain relations can be written in the form:

$$\sigma_{ij}(\mathbf{u}) = 2\mu_m \varepsilon_{ij}(\mathbf{u}^s) + \delta_{ij}(\lambda \nabla \cdot \mathbf{u}^s - \alpha M \xi), \quad (1)$$

$$p_f(\mathbf{u}) = -\alpha M \nabla \cdot \mathbf{u}^s + M\xi, \quad (2)$$

where $\varepsilon_{ij}(\mathbf{u}^s)$ is strain tensor of the solid, μ_m is the dry-rock (matrix or frame) shear modulus, and

$$\lambda = K_G - \frac{2}{d_e}\mu_m, \quad (3)$$

is the Lamé parameter. Moreover, K_G is the Gassmann modulus given by

$$K_G = K_m + \alpha^2 M, \quad (4)$$

where

$$\alpha = 1 - \frac{K_m}{K_s}, \quad (5)$$

$$M = \left(\frac{\alpha - \phi}{K_s} + \frac{\phi}{K_f}\right)^{-1}; \quad (6)$$

K_s is the solid-grain bulk modulus, K_f is the fluid bulk modulus, and K_m is the dry-rock bulk modulus (e.g., Carcione, 2007). The parameter α is known as the Biot-Willis coefficient of the bulk material.

Let us consider an open-bounded domain $\Omega \subset R^2$ ($d_e = 2$ in this work) of bulk material with boundary $\Gamma = \partial\Omega$. The bulk density is

$$\rho = (1 - \phi)\rho_s + \phi\rho_f, \quad (7)$$

where ρ_s is the density of the solid grains and ρ_f denote the density of the fluid. Let the positive definite matrix $\mathcal{P}$ and the nonnegative matrix $\mathcal{B}$ be defined by

$$\mathcal{P} = \begin{pmatrix} \rho I & \rho_f I \\ \rho_f I & gI \end{pmatrix}, \quad \mathcal{B} = \begin{pmatrix} 0I & 0I \\ 0I & bI \end{pmatrix}, \quad (8)$$

where I is the identity matrix. The coupling coefficients g and b take into account, respectively, the mass and viscous effects associated with dynamic interactions between the solid and fluid phases. They are given by the following equations:

$$b = \frac{\eta}{\kappa}, \quad g = \frac{\mathcal{T}\rho_f}{\phi}, \quad \mathcal{T} = \frac{1}{2}\left(1 + \frac{1}{\phi}\right), \quad (9)$$

(Berryman, 1980), where η is the fluid viscosity, κ is the permeability, and $\mathcal{T}$ is known as the structure or tortuosity factor. Above a certain critical frequency ω_c the coefficients b and g become frequency dependent (Biot, 1956b; Carcione, 2007). This effect is associated with the departure of the flow from the laminar Poiseuille type at the pore scale, which occurs for angular frequencies greater than ω_c. The value of ω_c can be estimated as

$$\omega_c = \frac{\eta\phi}{\kappa\rho_f\mathcal{T}}. \quad (10)$$

Next, let $\mathcal{L}(\mathbf{u})$ be the second-order differential operator defined by

$$\mathcal{L}(\mathbf{u}) = (\nabla \cdot \sigma(\mathbf{u}), -\nabla p_f(\mathbf{u}))^{\mathsf{T}},$$

where T denotes transpose. Then if $\omega = 2\pi f$ is the angular frequency and $\mathbf{F}(\mathbf{x},\omega) = (\mathbf{F}^s(\mathbf{x},\omega), \mathbf{F}^f(\mathbf{x},\omega))$, and $\mathbf{x} \in \boldsymbol{\Omega}$ is the external source, the equations of motion as stated in the space-frequency domain are (Biot, 1956a, b),

$$-\omega^2\mathcal{P}\mathbf{u}(\mathbf{x},\omega) + i\omega\mathcal{B}\mathbf{u}(\mathbf{x},\omega) - \mathcal{L}(\mathbf{u}(\mathbf{x},\omega)) = \mathbf{F}(\mathbf{x},\omega), \quad \mathbf{x} \in \Omega. \quad (11)$$

To completely define our differential model we have to state the absorbing boundary condition. Let us denote by $\boldsymbol{\nu}$ the unit outer normal on Γ. Let $\boldsymbol{\chi}$ be a unit tangent on Γ so that $\{\boldsymbol{\nu}, \boldsymbol{\chi}\}$ is an orthonormal system on Γ. We will consider the solution of equation 11 in the 2D case with the following absorbing boundary condition

$$-\mathcal{G}_\Gamma(\mathbf{u}(\mathbf{x},\omega)) = i\omega\mathcal{D}S_\Gamma(\mathbf{u}(\mathbf{x},\omega)), \quad \mathbf{x} \in \Gamma, \quad (12)$$

where

$$\mathcal{G}_\Gamma(\mathbf{u}) = (\sigma(\mathbf{u})\boldsymbol{\nu} \cdot \boldsymbol{\nu}, \sigma(\mathbf{u})\boldsymbol{\nu} \cdot \boldsymbol{\chi}, p_f(\mathbf{u}))^{\mathsf{T}},$$
$$S_\Gamma(\mathbf{u}) = (\mathbf{u}^s \cdot \boldsymbol{\nu}, \mathbf{u}^s \cdot \boldsymbol{\chi}, \mathbf{u}^f \cdot \boldsymbol{\nu})^{\mathsf{T}}. \quad (13)$$

The matrix $\mathcal{D}$ in equation 12 is positive definite, and in the 2D case it is given by the following relations: $\mathcal{D} = \mathcal{A}^{\frac{1}{2}}\mathcal{N}^{\frac{1}{2}}\mathcal{A}^{\frac{1}{2}}$, where $\mathcal{N} = \mathcal{A}^{-\frac{1}{2}}\mathcal{M}^{\frac{1}{2}}\mathcal{A}^{-\frac{1}{2}}$ and

$$\mathcal{A} = \begin{pmatrix} \rho & 0 & \rho_f \\ 0 & \rho - \dfrac{\rho_f^2}{g} & 0 \\ \rho_f & 0 & g \end{pmatrix}, \quad \mathcal{M} = \begin{pmatrix} \lambda + 2\mu_m & 0 & \alpha M \\ 0 & \mu_m & 0 \\ \alpha M & 0 & M \end{pmatrix}. \quad (14)$$

Our purpose is to find an approximate solution of equation 11 with the boundary condition 12 in a 2D layered domain Ω. It was shown by Biot (1956a, b) that this equation predicts, besides the presence of two classical compressional fast P- and S-waves, the existence of a second slow P-wave which shows a diffusion-type behavior. For example, in a porous rock saturated either by water or gas, the fast P-wave induces a pressure gradient between the gas patches and the water saturated parts of the material. This in turn generates fluid flow and slow Biot waves, which diffuse away from the gas-water interfaces and are responsible for the attenuation and velocity dispersion of the fast P-wave. However, the interpretation of this effect at a macroscopic scale is incomplete for different reasons. Geertsma and Smit (1961) showed that the dissipation factor ($1/Q$) of the fast P-wave can be approximated by that of a Zener model (Ben-Menahem and Singh, 1981) if the quality factor satisfies $Q > 5$. They obtained, for the frequency of the Zener relaxation peak, the expression,

$$f_B \approx \frac{\phi\eta\rho}{2\pi\kappa\rho_f(\rho\mathcal{T} - \phi\rho_f)}. \quad (15)$$

This equation shows that the peak moves towards the high frequencies with increasing viscosity and decreasing permeability. This means that, at low frequencies, the attenuation decreases with increasing viscosity (or decreasing permeability). This is in contradiction with experimental data (e.g., Jones, 1986). Another apparent drawback is that the macroscopic-flow mechanism underestimates the velocity dispersion and attenuation in rocks (e.g., Mochizuki, 1982; Dvorkin et al., 1995; Arntsen and Carcione, 2001). In further studies, White developed the mesoscopic-loss mechanism (White, 1975; White et al., 1975), in which attenuation and velocity disper-

sion have the proper dependence on frequency and the material parameters.

WHITE THEORY

In this section we present a short review of the White theory. Let us consider a periodic layered system composed of porous media 1 and 2 with thickness d_l, $l = 1,2$, and period $d_1 + d_2$. White et al. (1975) obtained the complex modulus for a P-wave traveling along the direction perpendicular to the stratification. It is given by

$$E = \left[\frac{1}{E_0} + \frac{2(r_2 - r_1)^2}{\mathrm{i}\omega(d_1 + d_2)(I_1 + I_2)} \right]^{-1}, \tag{16}$$

where

$$E_0 = \left(\frac{p_1}{E_{G_1}} + \frac{p_2}{E_{G_2}} \right)^{-1}, \tag{17}$$

with $p_l = d_l/(d_1 + d_2)$, $l = 1,2$. Omitting the subindex l for clarity, we have for each medium,

$$E_G = K_G + \frac{4}{3}\mu_m. \tag{18}$$

Moreover,

$$r = \frac{\alpha M}{E_G} \tag{19}$$

is the ratio of fast P-wave fluid tension to total normal stress,

$$I = \frac{\eta}{\kappa k} \coth\left(\frac{kd}{2} \right) \tag{20}$$

is an impedance related to the slow P-wave,

$$k = \sqrt{\frac{\mathrm{i}\omega\eta}{\kappa K_E}} \tag{21}$$

is the complex wavenumber of the slow P-wave, and

$$K_E = \frac{E_m M}{E_G} \tag{22}$$

is an effective modulus, with

$$E_m = K_m + \frac{4}{3}\mu_m \tag{23}$$

the dry-rock fast P-wave modulus.

Let us assume in the following analysis that the properties of the frame are the same in media 1 and 2, and that the contrast is the result of two different saturating fluids (for example, water and gas). The mesoscopic mechanism is the result of the presence of the Biot slow waves that diffuse away from the gas-water interfaces causing attenuation and velocity dispersion. The mesoscopic-scale length is intended to be much larger than the grain sizes but much smaller than the wavelength of the pulse. In a partially saturated rock, at low frequencies there is enough time for pore pressure to equilibrate at a constant value. The process of equilibration is governed by the diffusion equation and the diffusivity constant is $\gamma = \kappa K_E/\eta$. The critical fluid-diffusion relaxation length L is obtained by setting $|kL| = 1$, where k is the wavenumber equation 21. This gives a value of $L = \sqrt{\gamma/\omega}$. The fluid pressures will be equilibrated if L is comparable to the period of the stratification. However, when the frequency is sufficiently high (e.g., smaller diffusion lengths), there is not enough time for pressure equilibration and fluid flow effects can be ignored. In this circumstance, the layers of rock saturated by different fluid types will remain at different pressures.

The approximate transition frequency separating the relaxed and unrelaxed states (i.e., the approximate location of the relaxation peak) is

$$f_m = \frac{8\kappa_1 K_{E_1}}{\pi\eta_1 d_1^2} \tag{24}$$

(Dutta and Seriff, 1979; Carcione et al., 2003), where the subindex 1 refers to water for a layered medium alternately saturated with water and gas. Equation 24 indicates that the mesoscopic-loss mechanism moves toward the low frequencies with increasing viscosity and decreasing permeability, i.e., the opposite behavior of the Biot relaxation mechanism whose peak frequency is given by equation 15.

At low enough frequencies, the fluid pressure is uniform (isostress state) and the effective modulus of the pore fluid is given by Wood's law (Wood, 1955):

$$\frac{1}{K_f} = \frac{p_1}{K_{f_1}} + \frac{p_2}{K_{f_2}}. \tag{25}$$

It can be shown (e.g., Johnson, 2001) that $E(\omega = 0)$ is equal to the plane-wave modulus equation 18 for a fluid whose composite modulus is given by equation 25. On the other hand, at high frequencies, the pressure is not uniform but can be assumed to be constant within each phase. In such a situation, Hill's theorem (Hill, 1964) gives the high-frequency limit $E(\omega = \infty) = E_0$ (see equation 16).

Finally, it is important to recall that, besides the Biot and mesoscopic-loss mechanisms, scattering attenuation may occur. Carcione and Picotti (2006) discuss the significance of the mesoscopic loss at seismic frequencies and compare it with other mechanisms, such as scattering. This theory is only valid for wavelengths much larger than the layer thickness, where the scattering effects are not significant.

The numerical-simulation algorithm is given in the appendix. It is based on an iterative domain-decomposition 2D finite-element algorithm for solving Biot equations of motion in a parallel computer.

MATRIX AND FLUID PROPERTIES

We consider a 2D layered computational domain Ω of uniform porosity $\phi = 0.3$, permeability $\kappa = 1$ Darcy, and tortuosity factor $\mathcal{T} = 1$. The tortuosity factor is a dimensionless parameter of magnitude greater or equal to one, which depends on the geometry of the porous medium. The tortuosity is important at high frequencies, affecting mainly the velocity of the slow wave (e.g., Carcione, 2007). Since the complex modulus given by White's theory is independent of the tortuosity, we choose a value equal to one (Carcione, 1998).

Permeability is related to porosity by the Kozeny-Carman relation,

$$\kappa = \frac{B\phi^3 D^2}{(1-\phi)^2} \tag{26}$$

(Mavko et al., 1998), where D is the grain diameter ($D = 80$ μm for a sandstone) and $B = 0.003$. We use the model of Krief et al., (1990) to obtain the dry-rock moduli K_m and μ_m. The porosity dependence is consistent with the concept of critical porosity, since the moduli should be small above a certain value of the porosity (usually from 0.4 to 0.6). The moduli are given by

$$K_m = K_s(1-\phi)^{3/(1-\phi)},$$
$$\mu_m = K_m\mu_s/K_s, \tag{27}$$

where K_s and μ_s are the bulk and shear moduli of the solid grains. The material properties of the matrix are given in Table 1. The domain Ω is a square divided into two rectangular subdomains Ω_1 and Ω_2. We consider two cases. In case A we have

$$\Omega_1 = \{0 < x < 800\text{ m}, 0 < y < 8.8\text{ m}\}, \quad \Omega_2 = \{0 \le x < 800\text{ m}, 8.8 < y < 800\text{ m}\},$$

while in case B we have

$$\Omega_1 = \{0 < x < 320\text{ m}, 0 < y < 4.4\text{ m}\}, \quad \Omega_2 = \{0 \le x < 320\text{ m}, 4.4 < y < 320\text{ m}\}.$$

In both cases region Ω_1 is fully saturated with water, while region Ω_2 consists of horizontal layers of width 40 cm for case A and 20 cm for case B, alternately saturated with gas and water. The properties of the fluids depend on temperature and pressure, which in turn depend on depth z. We assume that the properties of water do not change significantly with depth, while the gas adiabatic bulk modulus and density can be calculated from the van der Waals equation (Friedman, 1963; Morse and Ingard, 1986). The material properties of the fluids, which correspond to those of water and methane (CH_4) at 1-km depth (Carcione and Picotti, 2006), are given in Table 1.

PHASE VELOCITY AND QUALITY FACTOR

The complex bulk modulus of equation 16 can be expressed as $E = |E|\exp(i\theta)$, where θ is the loss angle. We use the concept of complex velocity to obtain the phase velocity and loss angle as a function of angular frequency ω. If ρ is the bulk density of equation 7, the complex velocity v is defined by the relation $\bar{\rho}v^2 = E$, where $\bar{\rho} = p_1\rho_1 + p_2\rho_2$ is the averaged density. Then, the phase velocity and loss angle are given by

$$v_p = \left[\text{Re}\left(\frac{1}{v}\right)\right]^{-1} \tag{28}$$

and

$$\theta = \tan^{-1}\left[\frac{\text{Im}(v^2)}{\text{Re}(v^2)}\right], \tag{29}$$

where Re and Im denote real and imaginary parts, respectively. The relation between the loss angle and the standard definition of quality factor in viscoelasticity is $Q^{-1} = \tan\theta$. Figure 1 shows the corresponding phase velocities (a) and loss angles (b) for cases A and B. The relaxation frequency is lower when the period of the stratification is higher, corresponding to the frequency of about 20 Hz and 77 Hz for cases A and B, respectively. This is in agreement with equation 24, where d_1 is the thickness of the water-saturated layer. The maximum loss is the same for both cases, corresponding to a

Table 1. Material properties.

Matrix	Grain bulk modulus, K_s	37 GPa
	Grain shear modulus, μ_s	44 GPa
	Grain density, ρ_s	2650 kg/m^3
	Dry-rock bulk modulus, K_m	8 GPa
	Dry-rock shear modulus, μ_m	9.5 GPa
	Porosity, ϕ	0.3
	Permeability, κ	1 Darcy
	Tortuosity, $\mathcal{T}$	1
Water	Bulk modulus, K_f	2.25 GPa
	Density, ρ_f	1040 kg/m^3
	Viscosity, η	3 cP
Gas	Bulk modulus, K_f	0.012 GPa
	Density, ρ_f	78 kg/m^3
	Viscosity, η	0.15 cP

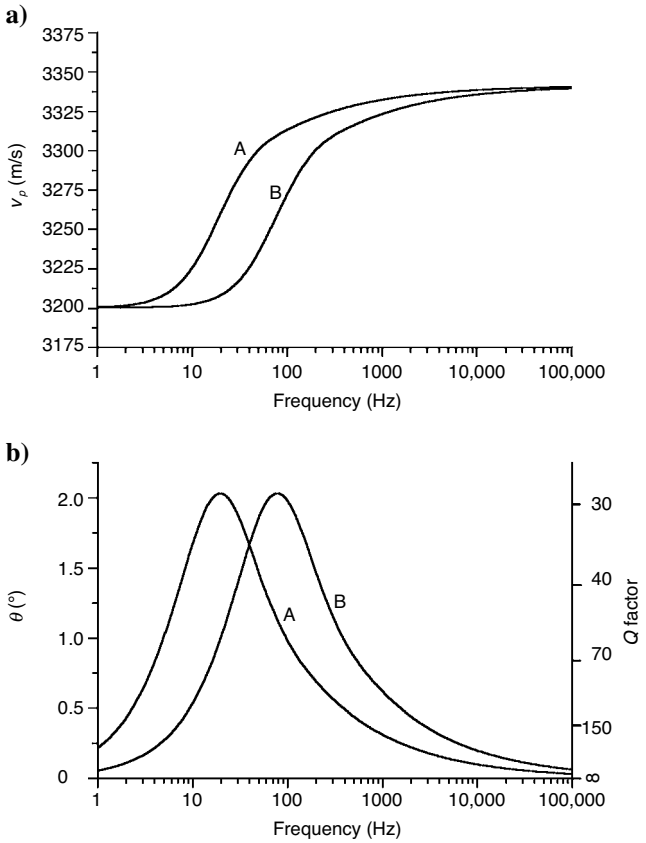

Figure 1. Phase velocity (a) and phase angle (and quality factor) (b), for sandstone saturated with water and gas for cases A and B. The material properties are shown in Table 1. The relaxation frequency is lower when the period of the stratification is higher (case A), in agreement with equation 24. The relaxation frequencies are nearly 20 Hz (case A) and 77 Hz (case B), while the maximum loss is the same for both cases, corresponding to a minimum value of Q of nearly 28.

minimum value of Q of about 28. These frequencies were chosen as the dominant frequencies of the source to be used in the simulations, which allowed us to better visualize the attenuation effects.

SIMULATIONS

The perturbation $(\mathbf{F}^s, \mathbf{F}^f)$ is a compressional point source applied to the matrix, located inside the region $\mathbf{\Omega}_1$ at $(x_s, y_s) = (400\text{ m}, 4\text{ m})$ for case A and at $(x_s, y_s) = (160\text{ m}, 4\text{ m})$ for case B. It has the form

$$\mathbf{F}^s(x, y, \omega) = \nabla \delta_{x_s, y_s} g(\omega), \quad \mathbf{F}^f = 0, \tag{30}$$

where δ_{x_s,y_s} denotes the Dirac distribution at (x_s, y_s). Also, $g(\omega)$ is the Fourier transform of the waveform

$$g(t) = -16 f_0^2 (t - t_0) e^{-8 f_0^2 (t - t_0)^2}, \tag{31}$$

with $t_0 = 1.25/f_0$, where the value f_0 was chosen such that the source central (dominant) frequency is equal to 20 Hz for case A and 77 Hz for case B.

A parallel iterative procedure is used to calculate the Fourier transforms of the matrix and fluid displacement vectors for 110 equally spaced frequencies in the interval (0, 60 Hz) for case A and (0, 242 Hz) for case B. The algorithm is implemented by using a uniform partition of Ω into squares of side length $h = 40$ cm for case A and $h = 20$ cm for case B. The numerical experiments were run in the IBM SP2 and the community cluster parallel computers at Purdue University under the MPI standard.

Figure 2 shows the time histories of the vertical component of the particle velocity (matrix) (a) and the corresponding frequency spectra (b) for the case A. The time histories correspond to seven receivers r_j $(j = 1, \ldots, 7)$, whose locations (x_{rj}, y_{rj}) are $x_{rj} = 400$ m $(j = 1, \ldots, 7)$ and $y_{r1} = 117$ m, $y_{r2} = 230$ m, $y_{r3} = 343$ m, $y_{r4} = 456$ m, $y_{r5} = 569$ m, $y_{r6} = 682$ m, and $y_{r7} = 795$ m.

Figure 3 shows the time histories of the vertical component of the particle velocity (matrix) (a) and the corresponding frequency spectra (b) for the case B. The time histories correspond to seven receivers r_j $(j = 1, \ldots, 7)$, whose locations (x_{rj}, y_{rj}) are $x_{rj} = 160$ m $(j = 1, \ldots, 7)$ and $y_{r1} = 49$ m, $y_{r2} = 94$ m, $y_{r3} = 139$ m, $y_{r4} = 189$ m, $y_{r5} = 229$, $y_{r6} = 274$ m, and $y_{r7} = 315$ m.

In both cases, the attenuation causes a reduction in the high frequency part of the spectrum, which become more consistent as the source-receiver distance increases. In order to give a clear picture of

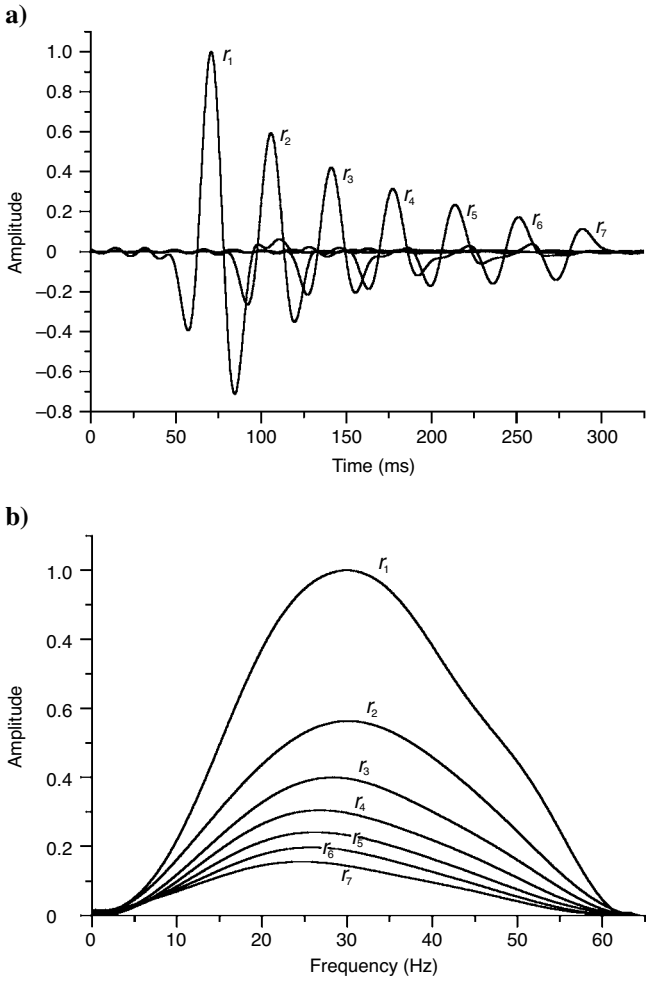

Figure 2. Time histories of the vertical component of the particle velocity (matrix) observed at the receivers r_j $(j = 1, \ldots, 7)$ (a) and corresponding frequency spectra (b) for the periodic gas-water saturated porous medium (case A).

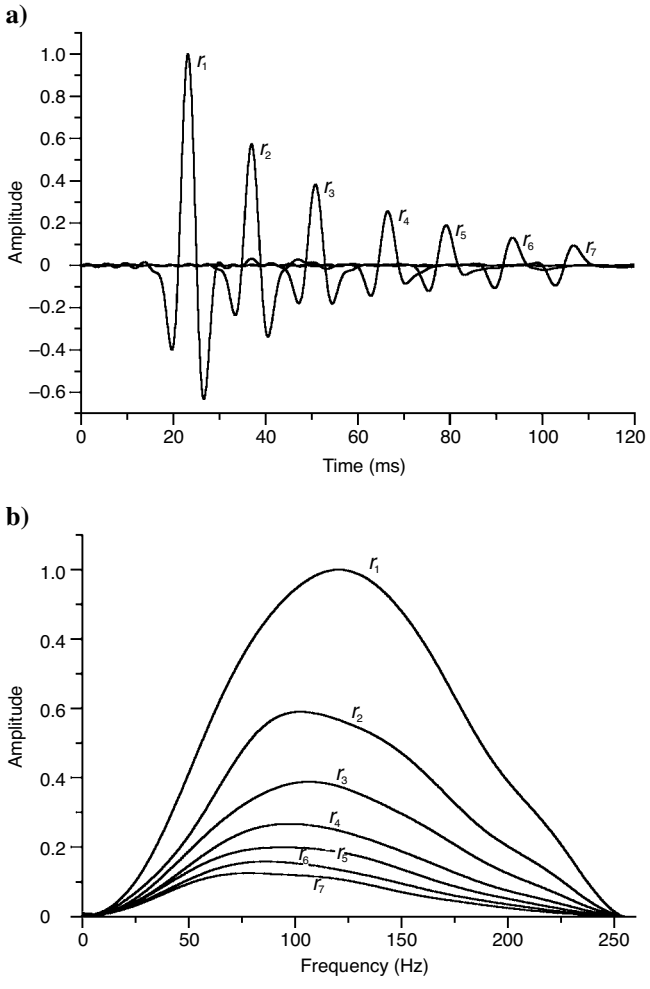

Figure 3. Time histories of the vertical component of the particle velocity (matrix) observed at the receivers r_j $(j = 1, \ldots, 7)$ (a) and corresponding frequency spectra (b) for the periodic gas-water saturated porous medium (case B).

the mesoscopic-loss effect, we also performed two other simulations in the model of case A, one considering a domain $\mathbf{\Omega}$ fully saturated with water and one with $\mathbf{\Omega}$ fully saturated with gas. In the following analysis we refer to these cases as homogeneous case A_W and homogeneous case A_G, respectively. The mesoscopic-loss effect is evident by comparing Figure 2 and Figure 4, where the time histories of the vertical component of the particle velocity (matrix) (a) and the corresponding frequency spectra (b) for the case A_W are shown.

Note that in this case the medium is practically lossless, because there is no loss of high frequencies, and the only attenuation effect is due to the geometrical spreading. The amplitude peaks corresponding to the arrival of the fast P-wave, observed both on the time histories and on the spectra, are higher than the corresponding peaks obtained using the periodic gas-water saturated medium (inhomogeneous case A). Moreover, the amplitude decay of the peaks is clearly lower than the corresponding decay observed in Figure 2 and Figure 3. This is due to the wave-induced flow occurring at the water-gas interfaces, which introduces an additional attenuation effect besides the geometrical spreading. The corresponding homogeneous case A_G is very similar to the case A_W, and the figure is not included here for brevity. Finally, Figure 5 shows the time histories of the vertical component of the particle velocity (matrix) at the receiver r_7, corresponding to the inhomogeneous case A and the homogeneous cases A_W and A_G.

This plot shows two different effects due to the velocity dispersion caused by the mesoscopic-loss mechanism: the delay in the arrival time of the pulse and the broadening of the pulse. In the case A, the wavelet arrives later and it is broader compared to the cases A_W and A_G. In order to give a quantitative evaluation of the attenuation, we estimate in the next section the quality factor Q from the time histories, to be compared with the value of Q obtained from White's theory.

ESTIMATION OF THE QUALITY FACTOR

To estimate the quality factor from the synthetic time histories we adopt two approaches (e.g., Picotti and Carcione, 2006): the classical spectral-ratio method and the frequency-shift method. Let $S(f)$ and $R(f)$ be the amplitude spectrum observed at the receivers r_i and r_j respectively, located at a distance d in the domain $\mathbf{\Omega}$. The spectral-ratio method is based on the property that, if the medium is homogeneous and the geometrical spreading factor G is frequency independent, the relationship between the logarithm of the spectral ratio and the frequency $f = \omega/2\pi$ is linear

$$\ln\left[\frac{S(f)}{R(f)}\right] = \left(\frac{\pi d}{v_p Q}\right) f + \ln G, \tag{32}$$

where v_p is the average phase velocity in the frequency band of interest. Since in our case the wavelength is large compared to the layer thickness, the medium may be considered homogeneous, and the velocity can be estimated by dividing the distances between the corresponding receivers by the traveltimes. Then, the quality factor Q can be determined from the slope of the line fitting $\ln(S(f)/R(f))$. The frequency-shift approach (Quan and Harris, 1997) is based on the property that, as the wave propagates through the medium, the high frequency part of the spectrum decreases faster than the low frequency part. This effect may be quantified by measuring the resulting downshift $\Delta f = f_S - f_R$, where f_S is the frequency centroid of $S(f)$ and f_R is the frequency centroid of $R(f)$. Then, if we approximate the spectrum $S(f)$ by a Gaussian with variance σ_s^2, we have

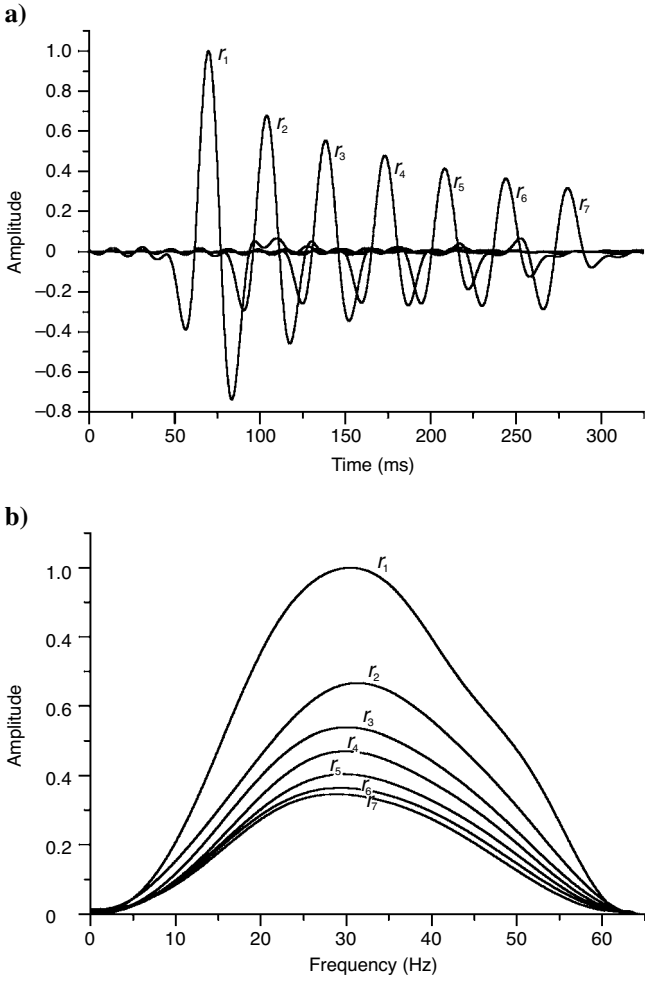

Figure 4. Time histories of the vertical component of the particle velocity (matrix) observed at the receivers r_j ($j = 1, \ldots, 7$) (a) and corresponding frequency spectra (b) for the water-saturated porous medium (homogeneous case A_W), to be compared with case A.

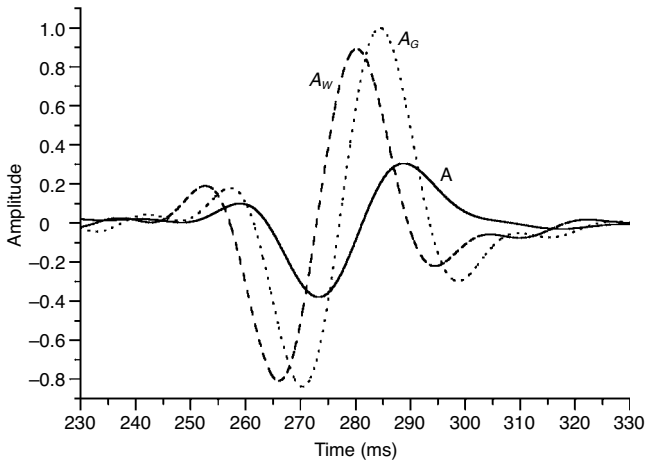

Figure 5. Time histories of the vertical component of the particle velocity (matrix) at receiver r_7, located at $x = 400$ m, $y = 795$ m for the periodic gas-water (case A) and the corresponding cases with full water saturation (homogeneous case A_W) and full gas saturation (homogeneous case A_G).

$$Q = \frac{\pi d \sigma_s^2}{v_p \Delta f}. \quad (33)$$

Picotti and Carcione (2006) develop a simple procedure to compensate for the presence of random noise in the seismic time histories, which is successfully used to remove the effect of numerical noise. Although these methods are applicable under the hypothesis of constant-Q in the bandwidth of interest (Dasgupta and Clark, 1998; Quan and Harris, 1997), the following considerations allowed us to also apply them to this particular case of frequency-dependent Q. The spectral-ratio method is more sensitive to this problem, resulting in noticeable departures of the logarithm of the spectral ratio from the linear trend. However, if we perform the analysis in a narrow frequency interval including the frequency centroids, we obtain a good approximation of the constant-Q condition. As an example, Figure 6 shows that, for case A, plotting the logarithm of the spectral ratio as a function of frequency in the interval $[\min(f_S - \sigma_S, f_R - \sigma_R), \max(f_S + \sigma_S, f_R + \sigma_R)]$ yields an approximate linear trend.

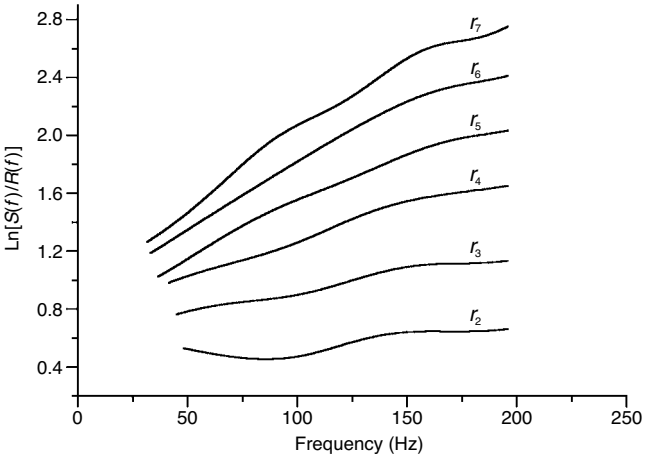

Figure 6. Logarithm of the spectral ratio $S(f)/R(f)$ as a function of frequency for case B, where $S(f)$ and $R(f)$ are the amplitude spectrum observed at the receivers r_1 and r_j $(j = 2, \ldots, 7)$, respectively.

Table 2. Estimation of Q for Case A. Deviations (%) between the theoretical $Q = 28$ using White theory and the estimated Q from the synthetic time histories using the frequency-shift and spectral-ratio methods. The value of Q is calculated for each pair of receivers r_1 and r_j $(j = 2,\ldots,7)$. The average deviation is 3.0% (frequency shift) and 4.2% (spectral ratio).

Receiver	Frequency-shift	Spectral-ratio
r_2	13.0	14.3
r_3	1.3	4.8
r_4	1.4	1.8
r_5	0.2	0.9
r_6	0.9	2.5
r_7	1.4	1.0

Table 3. Estimation of Q for Case B. Deviations (%) between the theoretical $Q = 28$ using White theory and the estimated Q from the synthetic time histories using the frequency-shift and spectral-ratio methods. The value of Q is calculated for each pair of receivers r_1 and r_j $(j = 2,\ldots,7)$. The average deviation is 2.1% (frequency shift) and 2.8% (spectral ratio).

Receiver	Frequency-shift	Spectral-ratio
r_2	5.0	5.8
r_3	2.8	3.9
r_4	1.6	1.3
r_5	1.5	3.2
r_6	1.7	2.2
r_7	0.2	0.5

On the other hand, the frequency-shift method is less sensitive to this problem when the spectrum of the signal is Gaussian, because the nonlinear trend of Q is more noticeable for very high and low frequencies (see Figure 1b). In this zone, the amplitude of the signal is low, resulting in small contributions in the integrals for the computation of variances and frequency centroids. Moreover, the noise removal procedure further attenuates this effect. Tables 2 and 3 show the percentage deviations between the estimated values of Q using the two methods and the theoretical Q derived from White's theory in equation 29. For both methods, the deviations increase with decreasing offsets, in agreement with the fact that the attenuation effects are generally observed with accuracy over large distances. For the case A, the average deviation is 3.0% using the frequency-shift method and 4.2% using the spectral-ratio method. For case B, the average deviation is 2.1% using the frequency-shift method and 2.8% using the spectral-ratio method. We conclude that these estimations of Q are in very good agreement with the theoretical value of the quality factor predicted by White ($Q = 28$ both for cases A and B).

CONCLUSIONS

We successfully tested a finite-element method to model the mesoscopic-loss mechanism, using a laminated medium consisting of porous layers alternately saturated with gas and water. The advantage of using this modeling algorithm is that the equation of motion is solved in the frequency domain. This allows us to implement any functional form of attenuation as a function of frequency, as for instance, general viscoelastic models and high-frequency visco-dynamic effects.

We used White's theory to predict the values of attenuation and velocity dispersion as a function of frequency in two different cases of partial saturation. The numerical experiments confirm the predictions of the theory, showing that the mechanism significantly affects the signals in the seismic band. Moreover, we estimated the quality factor from the synthetic time histories by using the spectral-ratio and frequency-shift methods, and found values that are in very good agreement with the theoretical values predicted by White's theory. The numerical experiments show that the finite-element algorithm has accurately modeled the attenuation effects, and thus, it can be used to describe this phenomenon in highly heterogeneous porous materials, such as the case of patchy saturation and fractal porosity-permeability distributions, where analytical solutions (with approximations) cannot be employed.

This study demonstrates that mesoscopic-scale heterogeneities highly affect the amplitude and phase of the seismic pulse at frequencies used in reservoir exploration. The attenuation and velocity dispersion are closely related to changes in saturation, permeability, and mineral properties. White's theory is a reference model to qualitatively evaluate the degree of loss, dispersion, and the location of the relaxation peak. Use of the present modeling algorithm allows us to study the phenomenon under realistic conditions, namely, statistical variations of the properties (e.g., fractal media), obtained, for instance, from outcrops or cores.

ACKNOWLEDGMENTS

This work was financed in part by the Norwegian Research Council through the Rock Seismic (ROSE) project at NTNU. It was also partially funded by CONICET, Argentina (PIP 5126/05) and the Agencia Nacional de Promoción Científica y Tecnológica (ANPCyT), PICT 2003, #03-13376. The authors are grateful to William Whitson and Bryan Putnam from Purdue University Computing Center for their technical support. We thank Robert J. Ferguson for a very detailed and constructive review.

APPENDIX A

THE MODELING ALGORITHM

An iterative wave propagation domain-decomposition algorithm is presented in this section. In order to represent the attenuation effect due to wave-induced fluid flow in the seismic frequency range, we perform a numerical simulation of wave propagation in a 2D layered domain $\mathbf{\Omega}$ by using the Biot equations of motion, equations 11, under the boundary condition, equation 12. This requires the solution of a huge linear system of equations, due to the large number of degrees of freedom needed to properly discretize the physical model, because the size of the local heterogeneities is much smaller than the wavelengths in the frequency range being analyzed. Because the associated algebraic problem is complex valued and noncoercive, no known efficient iterative global solvers can be employed (Brenner and Scott, 1994; Ha et al., 2002). To tackle this difficulty, a parallel iterative domain-decomposition algorithm is developed. The algorithm uses a nonconforming rectangular element (Douglas et al., 1999) to approximate the displacement vector in the solid phase, while the displacement in the fluid phase is approximated using the vector part of the Raviart-Thomas-Nedelec mixed finite-element space of zero order, which is a conforming space (Raviart and Thomas, 1975; Nedelec, 1980).

Let us consider a nonoverlapping partition of $\mathbf{\Omega}$ into N rectangular subdomains $\mathbf{\Omega}_j$ such that $\mathbf{\Omega} = \cup_{j=1}^{N} \mathbf{\Omega}_j$. The finite-element spaces will be defined locally on a reference square $\hat{R} = [-1,1]^2$ as follows. For each component of the solid displacement vector, set

$$\widehat{\mathcal{NC}}(\hat{R}) = \text{Span}\{1,\hat{x},\hat{y},\zeta(\hat{x}) - \zeta(\hat{y})\}, \quad \zeta(\hat{x}) = \hat{x}^2 - \frac{5}{3}\hat{x}^4,$$

with the degrees of freedom being the values at the midpoint of each edge of $\hat{R}$. Moreover, for the fluid displacement vector set

$$\hat{\mathcal{W}}(\hat{R}) = \text{Span}\{(\psi^L(\hat{x}),0)^{\mathsf{T}},(\psi^R(\hat{x}),0)^{\mathsf{T}},(0,\psi^B(\hat{y}))^{\mathsf{T}},$$
$$(0,\psi^T(\hat{y}))^{\mathsf{T}}\},$$

where T denotes transpose,

$$\psi^L(\hat{x}) = \frac{-1+\hat{x}}{2}, \quad \psi^R(\hat{x}) = \frac{1+\hat{x}}{2},$$
$$\psi^B(\hat{y}) = \frac{-1+\hat{y}}{2}, \quad \psi^T(\hat{y}) = \frac{1+\hat{y}}{2}.$$

Figure A-1 shows the local degrees of freedom (dofs) associated with each component of the solid displacement and the fluid displacement vector.

Now, the local finite-element spaces associated with the partition $\mathbf{\Omega}$ are defined by scaling and translations in the usual fashion as follows. For each $\mathbf{\Omega}_j$, let $F_{\mathbf{\Omega}_j}:\hat{R}\rightarrow\mathbf{\Omega}_j$ be an invertible affine mapping such that $F_{\mathbf{\Omega}_j}(\hat{R}) = \mathbf{\Omega}_j$, and define

$$\mathcal{NC}_j^h = \{\mathbf{v} = (v_1,v_2)^{\mathsf{T}}: v_i = \hat{v}_i \circ F_{\mathbf{\Omega}_j}^{-1}, \hat{v}_i \in \widehat{\mathcal{NC}}(\hat{R}), i = 1,2\},$$

$$\mathcal{W}_j^h = \{\mathbf{w}: \mathbf{w} = \hat{\mathbf{w}} \circ F_{\mathbf{\Omega}_j}^{-1}, \hat{\mathbf{w}} \in \hat{\mathcal{W}}(\hat{R})\},$$

where $\circ$ denotes the function composition.

Set $\Gamma_j = \partial\mathbf{\Omega} \cap \partial\mathbf{\Omega}_j$, $\Gamma_{jk} = \partial\mathbf{\Omega}_j \cap \partial\mathbf{\Omega}_k$, and denote by $\boldsymbol{\nu}_{jk}$ the unit outer normal on Γ_{jk} from $\mathbf{\Omega}_j$ to $\mathbf{\Omega}_k$ and by $\boldsymbol{\nu}_j$ the unit outer normal to Γ_j. Let $\boldsymbol{\chi}_j$ and $\boldsymbol{\chi}_{jk}$ be two unit tangents on Γ_j and Γ_{jk} so that $\{\boldsymbol{\nu}_j,\boldsymbol{\chi}_j\}$ and $\{\boldsymbol{\nu}_{jk},\boldsymbol{\chi}_{jk}\}$ are orthonormal systems on Γ_j and Γ_{jk}, respectively.

Consider the decomposition of problem equations 11 and 12 over $\mathbf{\Omega}_j$ as follows: for $j = 1,\ldots,N$, find $\mathbf{u}_j(x,\omega)$ satisfying

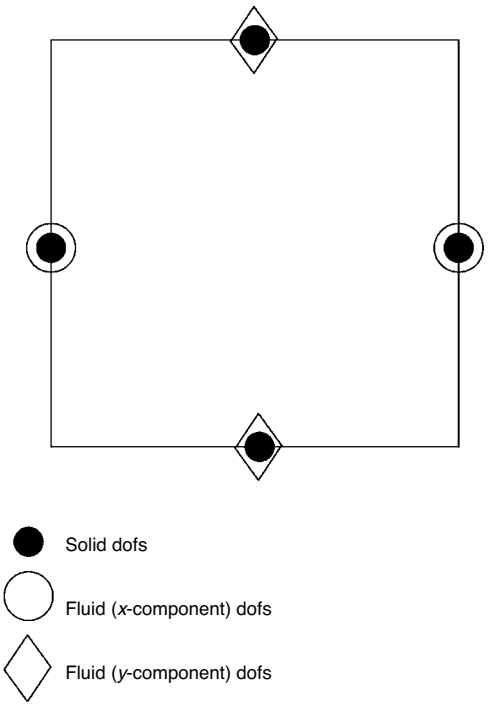

Figure A-1. Local degrees of freedom (dofs) associated with each component of the solid displacement and the fluid displacement vector.

$$-\omega^2\mathcal{P}\mathbf{u}_j + i\omega\mathcal{B}\mathbf{u}_j - \mathcal{L}(\mathbf{u}_j) = \mathbf{F}, \quad \mathbf{u}_j \in \mathbf{\Omega}_j, \quad \text{(A-1)}$$

$$\mathcal{G}_{\Gamma_{jk}}(\mathbf{u}_j) + i\omega\beta_{jk}S_{\Gamma_{jk}}(\mathbf{u}_j) = \mathcal{G}_{\Gamma_{kj}}(\mathbf{u}_k) - i\omega\beta_{jk}S_{\Gamma_{kj}}(\mathbf{u}_k), \quad \mathbf{u}_j,\mathbf{u}_k \in \Gamma_{jk}, \quad \text{(A-2)}$$

$$-\mathcal{G}_{\Gamma_j}(\mathbf{u}_j) = i\omega\mathcal{D}S_{\Gamma_j}(\mathbf{u}_j), \quad \mathbf{u}_j \in \Gamma_j, \quad \text{(A-3)}$$

where $\mathcal{G}_{\Gamma_{jk}}$ and $\mathcal{G}_{\Gamma_j}$ are defined as in equation 13 and β_{jk} is a positive definite matrix function defined on the interior boundaries Γ_{jk}. The Robin transmission conditions A-2 impose the continuity of the solid displacement, the normal component of the fluid displacement and the stresses at the interior interfaces Γ_{jk}.

Next, following Douglas et al. (1999) and Santos and Sheen (2007), let us introduce a set of Lagrange multipliers λ^h_{jk} associated with the values of the forces at the midpoints ξ_{jk} of Γ_{jk} in the sense that $\lambda^h_{jk} \sim \mathcal{G}_{jk}(\mathbf{u}_j)(\xi_{jk})$. The Lagrange multipliers λ^h_{jk} belong to the following space of functions defined on the interior interfaces Γ_{jk}:

$$\Lambda^h = \{\lambda^h : \lambda^h|_{\Gamma_{jk}} = \lambda^h_{jk} \in [P_0(\Gamma_{jk})]^3 = \Lambda^h_{jk}, \ \forall \ \{j,k\}\},$$

where $P_0(\Gamma_{jk})$ denotes the constant functions on Γ_{jk}.

In order to define our iterative domain decomposition procedure we need to introduce some notation. For $X \subset R^2$ with boundary ∂X, let $(\cdot,\cdot)_X$ and $\langle\cdot,\cdot\rangle_{\partial X}$ denote the complex $L^2(X)$ and $L^2(\partial X)$ inner products for scalar, vector, or matrix valued functions. Moreover, for $\Gamma = \Gamma_j$ or $\Gamma = \Gamma_{jk}$ let $\langle\langle u,v\rangle\rangle_\Gamma$ denote the approximation of $\langle\cdot,\cdot\rangle_\Gamma$ by the midpoint quadrature: $\langle\langle u,v\rangle\rangle_\Gamma = (u\bar{v})(\xi_{jk})|\Gamma|$ where $|\Gamma|$ is the measure of Γ.

The domain-decomposition iteration is defined as follows: For all $j = 1,\ldots,J$, choose an initial value $(\mathbf{u}_j^{\{h,0\}}, \lambda_{jk}^{\{h,0\}}) \in \mathcal{NC}_j^h \times \mathcal{W}_j^h \times \Lambda_{jk}^h$. Then, for $n = 1,2,3,\ldots$, and $j = 1,\ldots,J$, compute $(\mathbf{u}_j^{\{h,n\}}, \lambda_{jk}^{\{h,n\}}) \in \mathcal{NC}_j^h \times \mathcal{W}_j^h \times \Lambda_{jk}^h$ as the solution of the equations

$$\begin{aligned}
&-\omega^2(\mathcal{P}\mathbf{u}_j^{\{h,n\}},\mathbf{v})_{\mathbf{\Omega}_j} + i\omega(\mathcal{B}\mathbf{u}_j^{\{h,n\}},\mathbf{v})_{\mathbf{\Omega}_j} \\
&\quad + \sum_{l,m}(\sigma_{lm}(\mathbf{u}_j^{\{h,n\}}),\varepsilon_{lm}(\mathbf{v}^{(1)}))_{\mathbf{\Omega}_j} \\
&\quad - (p_f(\mathbf{u}_j^{\{h,n\}}),\ \nabla\ \cdot\mathbf{v}^{(2)}))_{\mathbf{\Omega}_j} + i\omega\langle\mathcal{D}S_{\Gamma_j}(\mathbf{u}_j^{\{h,n\}}),S_{\Gamma_j}(\mathbf{v})\rangle_{\Gamma_j} \\
&\quad + \sum_k \langle\langle i\omega\beta_{jk}\mathcal{S}_{\Gamma_{jk}}(\mathbf{u}_j^{\{h,n\}}),\mathcal{S}_{\Gamma_{jk}}(\mathbf{v})\rangle\rangle_{\Gamma_{jk}} \\
&= (\mathbf{F},\mathbf{v})_{\mathbf{\Omega}_j} - \sum_k \langle\langle i\omega\beta_{jk}\mathcal{S}_{\Gamma_{jk}}(\mathbf{u}_k^{\{h,n-1\}}),\mathcal{S}_{\Gamma_{jk}}(\mathbf{v})\rangle\rangle_{\Gamma_{jk}} \\
&\quad + \sum_k \langle\langle\lambda_{kj}^{\{h,n-1\}},\mathcal{S}_{\Gamma_{jk}}(\mathbf{v})\rangle\rangle_{\Gamma_{jk}}, \\
&\quad \mathbf{v}(\mathbf{v}^{(1)},\mathbf{v}^{(2)}) \in \mathcal{NC}^h(\Omega_j) \times \mathcal{W}_j^h, \qquad \text{(A-4)}
\end{aligned}$$

$$\lambda_{jk}^{\{h,n\}} = \lambda_{kj}^{\{h,n-1\}} - i\omega\beta_{jk}[S_{\Gamma_{jk}}(\mathbf{u}_j^{\{h,n\}}) + S_{\Gamma_{kj}}(\mathbf{u}_k^{\{h,n-1\}})](\xi_{jk}), \quad \text{on } \Gamma_{jk}, \ \forall\ k. \qquad \text{(A-5)}$$

Equation A-5 is used to update the Lagrange multipliers. This equation imposes the continuity of the solid displacement components at the mid-points ξ_{jk} of the interior interfaces Γ_{jk} after convergence has been achieved.

Equation A-4 yields a 12×12 linear system of equations for the degrees of freedom associated with the vector displacements of the solid and fluid phases on each subdomain $\mathbf{\Omega}_j$ at the n-iteration level. The iteration A-4 and A-5 is a Jacobi-type iteration that converges to the solution of equations 11 and 12 (Santos and Sheen, 2007). An iteration twice as fast may also be defined by using a red-black type iteration (Douglas et al., 2001; Ha et al., 2002; Santos and Sheen, 2007). The iteration parameter matrix β_{jk} is chosen to have the same form of the matrix $\mathcal{D}$ in equation 12, with entries obtained by averaging the coefficients in the definition of the matrices $\mathcal{A}$ and $\mathcal{M}$ in equation 14 on both sides of the boundary Γ_{jk}. The space-time solution is obtained by solving A-4 for a finite number of temporal frequencies and using an approximate inverse Fourier transform (Douglas et al., 1993).

For clarity, a list of mathematical symbols can be found at http://en.wikipedia.org/wiki/Table_of_mathematical-symbols

REFERENCES

Arntsen, B., and J. M. Carcione, 2001, Numerical simulation of the Biot slow wave in water-saturated Nivelsteiner sandstone: Geophysics, **66**, 890–896.

Ben-Menahem, A., and S. G. Singh, 1981, Seismic waves and sources: Springer-Verlag.

Berryman, J. G., 1980, Confirmation of Biot's theory: Applied Physics Letters, **33**, 382–384.

Biot, M. A., 1956a, Theory of propagation of elastic waves in a fluid-saturated porous solid. I. Low frequency range: Journal of the Acoustical Society of America, **28**, 168–171.

———, 1956b, Theory of propagation of elastic waves in a fluid-saturated porous solid. II. Higher frequency range: Journal of the Acoustical Society of America, **28**, 179–191.

———, 1962, Mechanics of deformation and acoustic propagation in porous media: Journal of Applied Physics, **33**, 1482–1498.

Brenner, S. C., and L. R. Scott, 1994, The mathematical theory of finite element methods: Springer-Verlag.

Cadoret, T., D. Marion, and B. Zinszner, 1995, Influence of frequency and fluid distribution on elastic wave velocities in partially saturated limestones: Journal of Geophysical Research, **100**, 9789–9803.

Carcione, J. M., 1998, Viscoelastic effective rheologies for modeling wave propagation in porous media: Geophysical Prospecting, **46**, 249–270.

———, 2007, Wave fields in real media: Wave propagation in anisotropic, anelastic, porous, and electromagnetic media: Handbook of Geophysical Exploration, **38**, Elsevier (2nd ed., revised and extended).

Carcione, J. M., H. B. Helle, and N. H. Pham, 2003, White's model for wave propagation in partially saturated rocks: Comparison with poroelastic numerical experiments: Geophysics, **68**, 1389–1398.

Carcione, J. M., and S. Picotti, 2006, P-wave seismic attenuation by slow-wave diffusion: Effects of inhomogeneous rock properties: Geophysics, **71**, no. 3; O1–O8.

Chin, R. C. Y., J. G. Berryman, and G. W. Hedstrom, 1985, Generalized ray expansion for pulse propagation and attenuation in fluid-saturated porous media: Wave Motion, **7**, 43–66.

Dasgupta, R., and R. A. Clark, 1998, Estimation of Q from surface seismic reflection data: Geophysics **63**, 2120–2128.

Diallo, M. S., M. Prasad, and E. Appel, 2003, Comparison between experimental results and theoretical predictions for P-wave velocity and attenuation at ultrasonic frequency: Wave Motion, **37**, 1–16.

Douglas, J. Jr., J. E. Santos, and D. Sheen, 2001, Nonconforming Galerkin methods for the Helmholtz equation: Numerical Methods for Partial Differential Equations, **17**, 475–494.

Douglas, J. Jr., J. E. Santos, D. Sheen, and L. Bennethum, 1993, Frequency domain treatment of one-dimensional scalar waves: Mathematical Models and Methods in Applied Sciences, **3**, 171–194.

Douglas, J. Jr., J. E. Santos, D. Sheen, and X. Ye, 1999, Nonconforming Galerkin methods based on quadrilateral elements for second-order elliptic problems: RAIRO Mathematical Modeling and Numerical Analysis (M2AN), **33**, 747–770.

Dutta, N. C., and H. Odé, 1979a, Attenuation and dispersion of compressional waves in fluid-filled porous rocks with partial gas saturation (White model) — Part I: Biot theory: Geophysics, **44**, 1777–1788.

———, 1979b, Attenuation and dispersion of compressional waves in fluid-filled porous rocks with partial gas saturation (White model) — Part II: Results: Geophysics, **44**, 1789–1805.

Dutta, N. C., and A. J. Seriff, 1979, On White's model of attenuation in rocks

with partial saturation: Geophysics, **44**, 1806–1812.
Dvorkin, J., G. Mavko, and A. Nur, 1995, Squirt flow in fully saturated rocks: Geophysics, **60**, 97–107.
Friedman, A. S., 1963, Pressure-volume-temperature relationships of gases, virial coefficients: *in* American Institute of Physics Handbook: McGraw-Hill Book Co.
Geertsma, J., and D. C. Smit, 1961, Some aspects of elastic wave propagation in fluid-saturated porous solids: Geophysics, **26**, 169–181.
Gelinsky, S., and S. A. Shapiro, 1997, Dynamic-equivalent medium approach for thinly layered saturated sediments: Geophysical Journal International, **128**, F1–F4.
Gurevich, B., and S. L. Lopatnikov, 1995, Velocity and attenuation of elastic waves in finely layered porous rocks: Geophysical Journal International, **121**, 933–947.
Gurevich, B., V. B. Zyrianov, and S. L. Lopatnikov, 1997, Seismic attenuation in finely layered porous rocks: Effects of fluid flow and scattering: Geophysics, **62**, 319–324.
Ha, T., J. E. Santos, and D. Sheen, 2002, Nonconforming finite element methods for the simulation of waves in viscoelastic solids: Computer Methods in Applied Mechanics Engineering, **191**, 5647–5670.
Helle, H. B., N. H. Pham, and J. M. Carcione, 2003, Velocity and attenuation in partially saturated rocks — Poroelastic numerical experiments: Geophysical Prospecting, **51**, 551–566.
Hill, R., 1964, Theory of mechanical properties of fiber-strengthened materials: Journal of Mechanics and Physics of Solids, **11**, 357–372.
Johnson, D. L., 2001, Theory of frequency dependent acoustics in patchy-saturated porous media: Journal of the Acoustical Society of America, **110**, 682–694.
Jones, T. D., 1986, Pore-fluids and frequency dependent-wave propagation rocks: Geophysics, **51**, 1939–1953.
Krief, M., J. Garat, J. Stellingwerff, and J. Ventre, 1990, A petrophysical interpretation using the velocities of P and S waves (full waveform sonic): The Log Analyst, **31**, 355–369.
Mavko, G., T. Mukerji, and J. Dvorkin, 1998, The rock physics handbook: tools for seismic analysis in porous media: Cambridge University Press.
Mochizuki, S., 1982, Attenuation in partially saturated rocks: Journal of Geophysical Research, **87**, 8598–8604.
Morse, P. M., and K. U. Ingard, 1986, Theoretical acoustics: Princeton University Press.
Müller, T. M., and B. Gurevich, 2004a, One-dimensional random patchy saturation model for velocity and attenuation in porous rocks: Geophysics, **69**, 1166–1172.
———, 2004b, Seismic attenuation and dispersion due to wave-induced flow in 3-D inhomogeneous porous rocks: 74th Annual International Meeting, SEG, Expanded Abstracts.
———, 2005, Wave-induced fluid flow in random porous media: Attenuation and dispersion of elastic waves: Journal of the Acoustical Society of America, **117**, 2732–2741.
Nedelec, J. C., 1980, Mixed finite elements in R^3: Journal of Numerical Mathematics, **35**, 315–341.
Norris, A. N., 1993, Low-frequency dispersion and attenuation in partially saturated rocks: Journal of Acoustical Society of America, **94**, 359–370.
O'Connell, R., and B. Budiansky, 1974, Seismic velocities in dry and saturated cracked solids: Journal of Geophysical Research, **79**, 5412–5426.
Picotti, S., and J. M. Carcione, 2006, Estimating seismic attenuation (Q) in the presence of random noise: Journal of Seismic Exploration, **15**, 165–181.
Plona, T. J., 1980, Observation of a second bulk compressional wave in a porous medium at ultrasonic frequencies: Applied Physics Letters, **36**, 259–261.
Pride, S. R., J. G. Berryman, and J. M. Harris, 2004, Seismic attenuation due to wave-induced flow: Journal of Geophysical Research, **109**, B01201; http://dx.doi.org/10.1029/2003JB002639.
Pride, S. R., E. Tromeur, and J. G. Berryman, 2002, Biot slow wave effects in stratified rock: Geophysics, **67**, 271–281.
Quan, Y., and J. M. Harris, 1997, Seismic attenuation tomography using the frequency shift method: Geophysics, **62**, 895–905.
Raviart, P. A., and J. M. Thomas, 1975, Mixed finite element method for 2nd-order elliptic problems: Mathematical Aspects of the Finite Element Methods: Lecture Notes of Mathematics, **606**, Springer.
Santos, J. E., and D. Sheen, 2007, Finite-element methods for the simulation of waves in composite saturated poroviscoelastic media: SIAM Journal of Numerical Analysis, **45**, 389–420.
Shapiro, S. A., and T. M. Müller, 1999, Seismic signatures of permeability in heterogeneous porous media: Geophysics, **64**, 99–103.
Smeulders, D. M. J., 2005, Experimental evidence for slow compressional waves: Journal of Engineering Mechanics, **131**, 908–917.
White, J. E., 1975, Computed seismic speeds and attenuation in rocks with partial gas saturation: Geophysics, **40**, 224–232.
White, J. E., N. G. Mikhaylova, and F. M. Lyakhovitskiy, 1975, Low-frequency seismic waves in fluid saturated layered rocks: Izvestija Academy of Sciences USSR, Physics of the Solid Earth, **11**, 654–659.
Wood, A. W., 1955, A textbook of sound: MacMillan Co.
Zyserman, F. I., P. M. Gauzellino, and J. E. Santos, 2003, Dispersion analysis of a non-conforming finite element method for the Helmholtz and elastodynamic equations: International Journal of Numerical Methods in Engineering, **58**, 1381–1395.